Research article

Elena Piacenza*, Alessandro Presentato, Belinda Heyne and Raymond J. Turner

Tunable photoluminescence properties of selenium nanoparticles: biogenic versus chemogenic synthesis

https://doi.org/10.1515/nanoph-2020-0239
Received April 18, 2020; accepted June 12, 2020

Abstract: Various technological and biomedical applications rely on the ability of materials to emit light (photoluminescence [PL]), and, among them, metal nanoparticles (NPs) and semi-conductor Quantum Dots (QDs) represent ideal candidates as sensing probes and imaging tools, portraying better PL features than conventional organic dyes. However, the knowledge of PL behavior of semiconductor NPs – i.e., selenium; SeNPs – is still in its infancy, especially for those synthesized by microorganisms. Considering the essential role played by biogenic SeNPs as antimicrobial, anticancer, and antioxidant agents, or food supplements, their PL properties must be explored to take full advantage of them as eco-friendly and versatile tools. Here, PL features of SeNPs produced by the Se-tolerant *Stenotrophomonas maltophilia* SeITE02 strain, compared with chemogenic ones, are investigated, highlighting the PL dependency on the NP size. Indeed, PL emission shifted from indigo-blue (emission wavelength λ_{em} 400–450 nm) to green-yellow (λ_{em} 480–570 nm) and orange-red (λ_{em} 580–700 nm) for small (ca. 50 nm) and big (ca. 100 nm) SeNPs respectively, revealing the versatility of an environmental bacterial isolate to synthesize diverse PL probes. Besides, biogenic SeNPs show PL lifetime comparable to those of the most used fluorophores, supporting their potential application as markers for (bio)imaging.

Keywords: biogenic selenium nanoparticles; fluorescence; photoluminescence; semiconductor nanoparticles; *stenotrophomonas*.

***Corresponding author: Elena Piacenza**, National Interuniversity Consortium of Materials Science and Technology (INSTM), Via G. Giusti, 9, 50121, Firenze, Italy, E-mail: elena.piacenza91@gmail.com
Alessandro Presentato: Department of Biological, Chemical and Pharmaceutical Sciences and Technologies (STEBICEF), University of Palermo, Viale delle Scienze Ed. 17, 90128, Palermo, Italy
Belinda Heyne: Department of Chemistry, University of Calgary, 2500 University Drive NW, Calgary, AB, Canada, T2N 1N4
Raymond J. Turner: Department of Biological Sciences, University of Calgary 2500 University Drive NW, Calgary, AB, Canada, T2N 1N4

1 Introduction

Microbial nanotechnology is an expanding research field based on the capability of microorganisms to sequester and/or transform non- or micro-essential yet toxic metal(-loid) ions into their less bioavailable elemental forms, which then assemble in either intra- or extra-cellular nanostructures (NSs) [1–2]. Among the broad spectrum of metal(loid) ionic species used as precursors for biogenic nanomaterial (NM) synthesis, those containing selenium (Se) – i.e., selenite (SeO_3^{2-}) and selenate (SeO_4^{2-}) – have gained particular interest, as they can be very toxic at relatively low concentrations, because of their mobility through the trophic chain and their tendency to bioaccumulate. In the past, bacteria have been used to remediate environmental matrices contaminated with Se compounds, attenuating their critical concentration and, simultaneously, producing selenium NSs (SeNSs), which can be recovered [3–7]. This aspect represents a technological advantage since Se is a scarce and rare element of our Earth's crust featuring properties (e.g., high photoconductivity, piezoelectricity, thermoelectricity, spectral sensitivity) [8–9] that makes it of utmost importance at an economic level. Indeed, its application greatly impacts manufacturing industries, export, and job opportunity creation; as an "energy-critical element", Se-based products are, for example, involved in renewable energy-based technologies [10–12].

Physical-chemical features of Se are strongly emphasized when it is scaled down to the nanorange (1–100 nm), where high surface-to-volume ratio, large surface energy, and spatial confinement arise, resulting in boosted catalytic, mechanical, electrical, optical, and magnetic properties as compared to the bulk materials [13]. However, the practical application of SeNMs is still held back by the lack of a complete understanding of their physical-chemical behavior as compared to other nanotechnological products, such as gold (Au) or silver (Ag) NSs. For instance, optical and photoluminescence (PL) properties of these metal NMs [14] can be exploited for the generation of sound

and innovative nanosensors and imaging markers, avoiding the need for additional fluorescent tags (proteins or dyes), which often leads to observational artifacts [15]. On this matter, metal or metal-based NSs have been studied in depth for their optical and PL features, yet this knowledge in the case of SeNSs is still lagging [6, 16–17]. Indeed, only few research groups started in the last 4 years to focus on the possibility to use chemogenic SeNSs for eukaryotic cell imaging, exploiting the ability of Se nanoproducts to emit light beyond the so-called biological window (300–500 nm), where cellular components (e.g., collagens and flavins) fluoresce, causing interference with most of the organic fluorescent compounds or Quantum Dots (QDs) [15–16]. Besides, the chemogenic SeNMs investigated so far seem to meet the criteria necessary for biomedical *in vitro* and *in vivo* applications, being biocompatible, biodegradable, and photostable [16], while organic fluorescent compounds or even QDs only partially satisfied these requirements [15].

Although a broad spectrum of chemogenic procedures has been developed to produce high-quality SeNSs, these processes mostly rely on dangerous operational conditions and the use of toxic reagents to obtain thermodynamically stable colloidal products [18], which is of fundamental importance for NM application. As opposed to conventional chemogenic syntheses, biogenic approaches give rise to thermodynamically stable yet structurally diverse SeNS products in a safe and *eco-friendly* manner, avoiding the need of post-production treatments [2]. To date, biogenic SeNMs were investigated for their applications in (i) biomedicine, as antimicrobial [19–27], anticancer [27–38] and antioxidant [27, 39–41] agents, due to their high biocompatibility towards eukaryotic *in vitro* and *in vivo* systems [22, 28, 40, 42], (ii) photocatalysis, and (iii) biosensing or pollutant adsorption [43–46], leaving still unveiled the potentiality of these NSs as a bioimaging tool. In particular, the PL properties of SeNPs produced by bacteria just recently began to be explored, as in the case of those recovered from the environmental isolate *Stenotrophomonas maltophilia* SeITE02 under metabolically controlled growth conditions [6]. Herein, the dependency of optical and PL properties on the size and shape of SeNPs synthesized by SeITE02 cells when grown in diverse complex media was studied, making a parallel with chemogenic SeNPs. In an attempt to support the application of these biogenic SeNPs as a relevant and valuable PL tool, PL lifetime measurements and Super Resolution-Confocal Laser Scanning Microscopy (SR-CLSM) were performed and duly discussed.

2 Experimental section

2.1 Materials and chemicals

Tryptone, yeast extract and Nutrient Broth (NB) powder were purchased from Oxoid™, while sodium chloride (NaCl, ACS grade), sodium selenite (Na_2SeO_3, ACS grade) and L-cysteine were obtained from Sigma-Aldrich®.

The 0.2 µm Filtropur, Carbon-coated Copper Grids (CF300-CU) and 200 µL Ultra-Micro cells used for either biogenic SeNP extract purification or characterization were purchased by Sarstedt, Electron Micorscopy Sciences and Hellma®, respectively.

2.2 Synthesis of biogenic and chemogenic SeNPs

The bacterial strain *Stenotrophomonas maltophilia* SeITE02, previously isolated from the rhizosphere of the Se-hyperaccumulator plant *Astragalus bisulcatus* [47] was used in the present study as a microbial cell factory for the synthesis of SeNPs. SeITE02 strain was routinely pre-cultured in either Luria Bertani (LB) [containing (g L^{-1}): NaCl (10), tryptone (10), yeast extract (5)] or NB [containing (g L^{-1}): Lab-Lemco powder (1), yeast extract (2), peptone (5), NaCl (5)] liquid-rich media for 16 h at 27 °C with shaking (150 rpm). The bacterial pre-cultures were subsequently inoculated for 48 h (1% v/v) in 250 mL Erlenmeyer flasks containing 50 mL of either LB or NB amended with 0.5 mM Na_2SeO_3 at 27 °C with shaking (150 rpm). The biogenic SeNP extracts were then recovered from SeITE02 cells following the procedure described elesewhere [6], while the organic material derived from SeNP extracts recovered from SeITE02 cells grown in either LB (OM_LB) or NB (OM_NB) were obtained through three centrifugation steps (12,000 *g* for 10 min), and the subsequent recovery of the SeNP-free supernatants.

Chemogenic SeNPs – henceforth indicated as L-cys SeNPs–were prepared as reported by Li et al. (2010) [48], where different Na_2SeO_3 (100 mM): L-cysteine (50 mM) molar ratios were applied – 1:3 or 1:4 – to obtain SeNPs comparable in average diameter (i.e., 50 or 100 nm) to those of biogenic synthesis. L-cys SeNPs_1:3 and L-cys SeNPs_1:4 were incubated for 16 h at room temperature in the presence of either OM_LB or OM_NB respectively, generating the samples L-cys SeNPs_1:3 + OM_LB and L-cys SeNPs_1:4 + OM_NB.

All the samples were stored at 4 °C prior to their use.

2.3 Transmission electron microscopy (TEM) imaging

Physical-chemical features of the Biogenic SeNP extracts, L-cys SeNPs, OMs and chemogenic SeNPs exposed to the OMs were investigated through a Hitachi H7650 TEM operating at 80 kV. The samples were prepared for TEM imaging as indicated elsewhere [49–50]. To establish the average diameter (expressed in nm with standard deviation) of either biogenic or chemogenic SeNPs, the actual size of 100 randomly chosen NPs was measured by using ImageJ software.

2.4 Optical and photoluminescence properties of biogenic SeNP extracts, chemogenic SeNPs, and OMs

Aliquots (200 µL) of either biogenic or chemogenic SeNP suspensions were used to study: (i) their optical properties (recording of absorbance spectra) through an Ocean Optics spectrophotometer and (ii) their PL features (emission and excitation spectra) exploiting a Varian Cary Eclipse fluorescence spectrophotometer with a 50 W Xenon lamp and a 4 nm excitation and emission band pass. The measurements were performed by varying excitation (λ_{exc}) and emission (λ_{em}) wavelengths according to the results derived from absorption spectroscopy. All the measurements were carried out on spectro-quality quartz cuvette with 10 mm path length.

2.5 Photoluminescence lifetime measurements of biogenic SeNP extracts and chemogenic SeNPs

Excited state lifetime measurements were collected in 200 µL aliquots of the recovered biogenic SeNP extracts and chemogenic SeNPs through an Edinburgh Instruments FLS900 using a Time-Correlated Single Photon Counting (TCSPC) *via* a MicroChannel Plate as a detection method, which determines the samples' decay curve after their excitation following a short laser pulse (ranging from 55 to 85 ps) [51]. The excitation was performed with either a 405 or 510 nm pulsed laser source with a repetition rate of 10 MHz (1/100 ns) and the set λ_{em} was matched to the results obtained from the steady-state emission spectra.

All the obtained data were subsequently analyzed through a deconvolution procedure and fitted based on a nonlinear least-squares error minimization method [52]. The measured PL decay $I(t)$ can be described as a multi-exponential fit:

$$I(t) = \sum a_i e^{(-t/\tau_i)}$$

where t is the temporal delay with respect to the light pulse, a_i is the pre-exponential factor and τ_i the lifetime of the ith component of PL decay [52]. For all the collected lifetime decays, two- or three-exponential fits were required to fit the data. The quality of the obtained fits was judged by considering the reduced χ^2 factors, where a good fit was defined when $1.1 < \chi^2 < 1.2$.

The intensity-weighted average PL lifetime of either biogenic or chemogenic SeNPs was subsequently calculated using the equation [52]:

$$<\tau> = \sum a_i \tau_i^2 / \sum a_i \tau_i$$

2.6 Super resolution-confocal laser scanning microscopy of biogenic SeNP extracts and chemogenic SeNPs

PL properties of SeNPs featuring 100 nm diameter (i.e., L-cys SeNPs_1:4 or Bio SeNP extract_NB) were further studied by air drying 20 µL sample on microscopy glass slides and imaged through a N-Storm SR-CLSM (Nikon® Instruments) by exploiting 405, 488 and 530-nm laser sources. The obtained SR-CLSM images were subsequently processed using IMARIS x64 software (Bitplane, Concord, MA, USA).

3 Results and discussion

3.1 Characterization of biogenic SeNP extracts and chemogenic SeNPs

SeITE02 cells grown in the presence of sodium selenite (Na_2SeO_3) – as Se precursor – and different complex media (Luria Bertani [LB] and nutrient broth [NB]) synthesized spherical SeNPs (Figures 1A, 2A), resembling in morphology those of chemical synthesis (Figures 1B, 2B), which were obtained through the reduction reaction occurring between L-cysteine and Na_2SeO_3 [48].

The complex media utilized influenced the size and polydispersity of the biogenic SeNPs. Indeed, SeITE02 LB-grown cells produced relatively monodisperse SeNPs, having ca. 45 nm as average diameter (Table 1, Figure 3A), while those generated by bacterial cells grown in NB were bigger (ca. 100 nm) (Table 1) and more polydisperse,

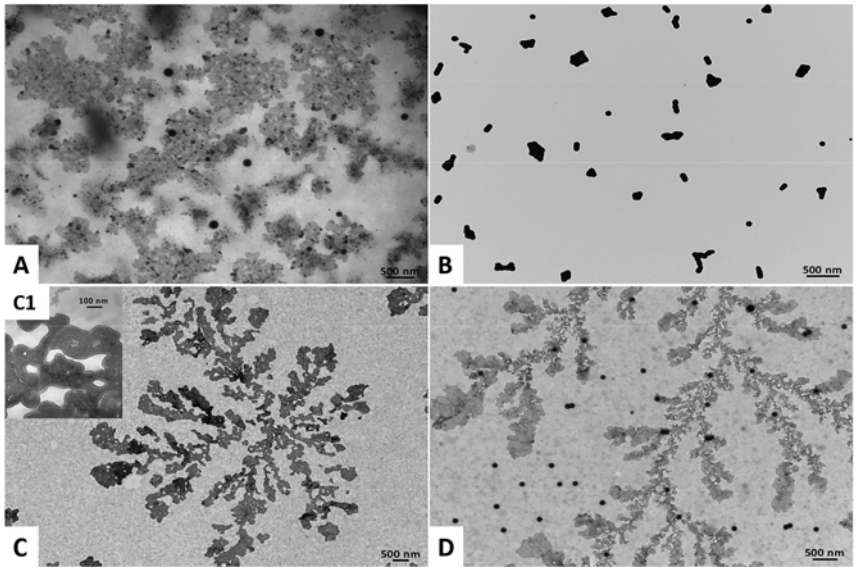

Figure 1: Transmission Electron Microscopy images of (A) Bio SeNP extract_LB, (B) L-cys SeNPs_1:3 (C) OM_LB, and (D) L-cys SeNPs_1:3 + OM_LB. The inlet (C1) shows a high magnification image of the OM_LB highlighting the presence of lipid-like vesicles.

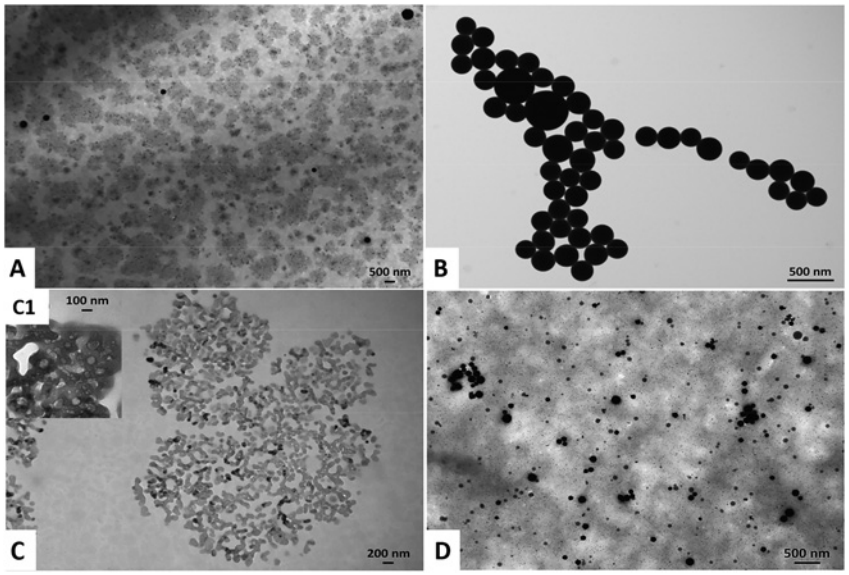

Figure 2: Transmission Electron Microscopy images of (A) Bio SeNP extract_NB, (B) L-cys SeNPs_1:4 (C) OM_NB, and (D) L-cys SeNPs_1:4 + OM_NB. The inlet (C1) shows a high magnification image of the OM_NB highlighting the presence of lipid-like vesicles.

having multiple NP populations ranging from 30 to 160 nm (Figure 3D).

Similar results were recently reported for the synthesis of AgNPs by *Klebsiella pneumoniae*, *Escherichia coli*, and *Pseudomonas jessinii*, as well as SeNPs produced by *Azospirillum brasilense*, where the authors recognized that differences in the composition of the growth media used strongly affected size and shape of the NPs [53–56]. In this regard, the meat extract present as "Lab-Lemco powder" in NB constituted an additional nutrient for SeITE02 cells, which was absent in LB. Therefore, the more complex composition and nutritional power of NB with the respect of LB may have influenced bacterial cells from a metabolic perspective, giving: (i) a less controlled and overall faster SeO_3^{2-} bioconversion, (ii) the occurrence of multiple nucleation events for NP growth, and (iii) the synthesis of SeNPs heterogeneous in size [55]. Considering the variation in size of biosynthesized SeNPs, for comparison, different Na_2SeO_3:L-cysteine ratios (1:3 and 1:4) [48] were used to obtain chemogenic NPs (L-cys SeNPs_1:3 and L-cys

Table 1: Average diameter of chemogenic and biogenic SeNPs.

SeNP samples	Average diameter (nm)
Bio SeNP extract_LB	45 ± 26
L-cys SeNPs_1:3	58 ± 19
L-cys SeNPs_1:3 + OM_LB	48 ± 8
Bio SeNP extract_NB	101 ± 29
L-cys SeNPs_1:4	99 ± 19
L-cys SeNPs_1:4 + OM_NB	57 ± 25

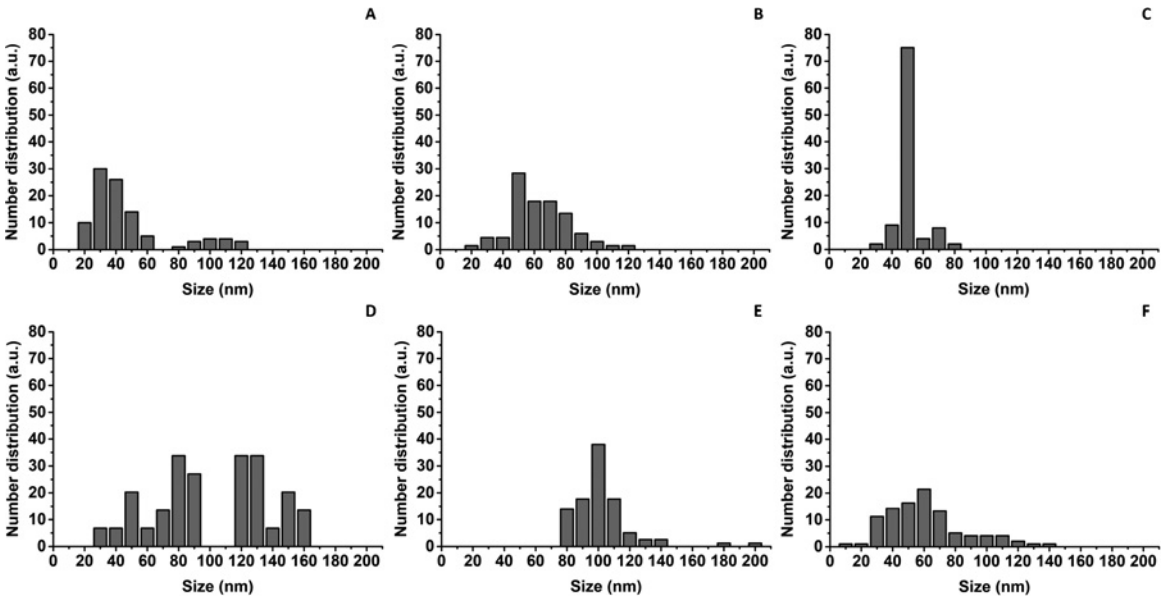

Figure 3: Size distribution of SeNPs within (A) Bio SeNP extract_LB, (B) L-cys SeNPs_1:3 (C) L-cys SeNPs_1:3 + OM_LB, (D) Bio SeNP extract_NB (E) L-cys SeNPs_1:4, and (F) L-cys SeNPs_1:4 + OM_NB.

SeNPs_1:4), having monodispersity and average diameters (i.e., ca. 58 and 99 nm) (Table 1) similar to biogenic ones (Figures 3B, 3E).

SeNPs within the biogenic extracts were also surrounded by a slightly electron-dense material (Figures 1A, 2A), which provided them strong thermodynamic stability, as NP aggregation was not detected up to two months of storage (4 °C) and upon air-drying of the samples on Transmission Electron Microscopy (TEM) grids. This observation is in line with earlier reports in the case of SeNSs produced by either SeITE02 [6] or other Gram-positive and negative environmental isolates [4–5, 7, 20, 24, 27]. Since previous investigations highlighted proteins and amphiphilic biomolecules as important components of SeNP extracts obtained from the same environmental isolate [6, 22–23, 57–59], it is reasonable to suggest a similar composition of the material surrounding the NPs in the present study, whose exact composition is behind the scope of this research. The latter is indicated as organic material (OM_LB or OM_NB). TEM imaging of the OMs further supported this hypothesis, showing electron-dense and organized structures (Figure 1C–C1, 2C–C1) that resembled, for their electron-transparency, lipid-like vesicles [6]. Conversely, chemogenic SeNPs revealed the tendency to agglomerate with each other (Figures 1B, 2B), likely due to the relatively low strength of L-cysteine to act as an electrostatic stabilizing agent, as also reported by Piacenza and colleagues [7]. This evidence, along with the thermodynamic stability gained by L-cys SeNPs after exposure to the OM isolated from the biogenic extracts (Table 1, Figures 1D, 2D), indicated the OM's fundamental role as an electrosteric stabilizer for NPs [2, 6, 23].

3.2 Optical properties of biogenic SeNP extracts and chemogenic SeNPs

Size and shape are two of the most crucial structural features of NMs that strongly influence their optical properties. Indeed, scaling down materials to the nanorange results in (i) an increased energy level spacing as the system becomes more and more confined, and (ii) the development, in noble metals, of surface plasmon resonance (SPR), which causes the displacement of NM surface electron cloud within the elemental conduction band from the nuclei, the consequent surface charge redistribution, and a precise *in phase*-coherent oscillation [14, 60]. This phenomenon generates a dipolar oscillation of electrons with a specific frequency, which mostly depends on size, shape and dielectric environment [14]. Although Se lacks of free conduction electrons, the light irradiation of SeNPs can cause exciton resonance or transition to occur [61–62], determining the development of unique optical properties of NPs. Furthermore, it has been reported how SeNPs exhibit various absorption behaviors, mostly because of the different synthetic procedures that give rise to a variety of final products in terms of size, shape, and surrounding optical environment, and, therefore, the quantum confinement effect, which is regulated by the NP average diameter [17].

Here, the optical properties of either biogenic or chemogenic SeNPs were strongly influenced by their size and polydispersity. A broad absorption band between 300 and 450 nm was detected for SeNPs of ca. 50 nm (i.e., Bio SeNP extract_LB, L-cys SeNPs_1:3, and L-cys SeNPs_1:3 + OM_LB), while those larger (i.e., Bio SeNP extract_NB, L-cys SeNPs_1:4, and L-cys SeNPs_1:4 + OM_NB) absorbed light in the 300–550 nm region (Figure 4). Since similar results were reported for both biogenic [34, 63–65] and chemogenic [18, 48, 66–69] SeNPs, this absorbance behavior can be ascribed to the presence of Se^0 at the nanoscale, whose exciton resonance effects are responsible for most of the light absorption phenomenon [61–62].

The broad absorption peak gradually descending towards the long-wavelength side of the spectrum detected for both biogenic and chemogenic NPs originates from (i) indirect interband and core electronic transitions (around 300 nm) [70], as well as (ii) coherent oscillations of excitons from one surface of SeNP to another, which generally determines a redshift of the exciton resonance peak as the NP size increases [70–71]. Indeed, the larger the NPs the less homogeneous will be their polarization determined by the incident light, leading to an increase of higher-order modes, whose exciton transition peaks are broader and at lower energies [71–72]. As a consequence, the maximum exciton resonance peak centered at ca. 300-340 nm in the case of small SeNPs (ca. 50 nm) (Figure 4A) redshifted towards ca. 520 nm for NPs with a diameter of 100 nm (Figure 4B), being in line with the results previously obtained for SeNPs produced by *Acinetobacter* sp. SW30 [34] and *Enterobacter* sp. strain [72]. This redshift is also responsible for the transition from orange to red color of the colloidal solutions [73]. Moreover, the presence of biomolecules (e.g., proteins, amino acid residues, cofactors, and secondary metabolites) [6, 57, 74] within the OMs able to absorb light [75] can account for the absorption in the 300–390 nm region, which is however significantly different from the absorption behavior of samples containing SeNPs (Figure 4). Thus, the absorption bands at 300–450 nm (Bio SeNP extract_LB, L-cys SeNPs_1:3, and L-cys SeNPs_1:3 + OM_LB) and 300–550 nm (Bio SeNP extract_NB, L-cys SeNPs_1:4, and L-cys SeNPs_1:4 + OM_NB) is here ascribed to the presence of SeNPs (Figure 4).

3.3 Photoluminescence properties and lifetime measurements of biogenic SeNP extracts and chemogenic SeNPs

Since PL of SeNPs has just recently gained scientific and applicative interest, the physical-chemical mechanisms responsible for this phenomenon, as well as its dependency on size, polydispersity, and the surrounding capping agents [16, 76], are still scarcely investigated. Here, PL emission of biogenic and chemogenic SeNPs was collected at different excitation wavelengths (λ_{excs}) based on the absorption spectra (Figure 4), being in the (i) 300–400 nm range for NPs of 50 nm (Bio SeNP extract_LB, L-cys SeNPs_1:3, and L-cys SeNPs_1:3 + OM_LB), and their corresponding OM_LB (Figure 5), or (ii) 300–500 nm range for those larger (Bio SeNP extract_NB, L-cys SeNPs_1:4, and L-cys SeNPs_1:4 + OM_NB), as well as OM_NB (Figure 6).

The origin and processes of light emission in NPs are vastly different in the case of metal, semiconductor, and insulator NMs [14], among which the first two groups are to date the most investigated and explored, given their ease of synthesis (e.g., control over size and morphology) and a broad range of applications. In metals, PL generally occurs due to the excitation of *d*-electrons to the *sp*-conduction band, which is followed by a radiative emission, whose efficiency is quite low due to the dominance of non-radiative processes within the system [14]. Since Se shares several physical-chemical properties with metals, the strong PL emission observed for both chemogenic and biogenic SeNPs (Figures 5, 6) could be partially ascribed to transitions from $3s^2p^6d^{10}$ bands – or lower energy level – to conduction – or higher – bands [70]. The excitation of chemogenic SeNPs at 300 nm, the wavelength at which

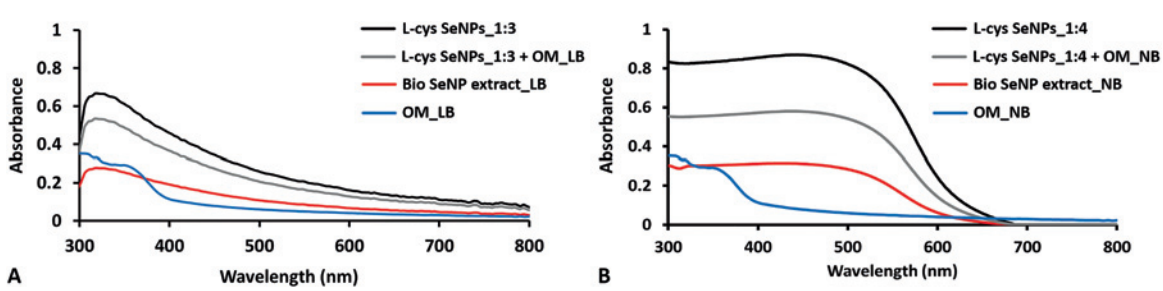

Figure 4: Absorbance spectra collected for samples containing SeNPs having ca. (A) 50 and (B) 100 nm as average diameter and their correspondent OM (i.e., OM_LB and OM_NB).

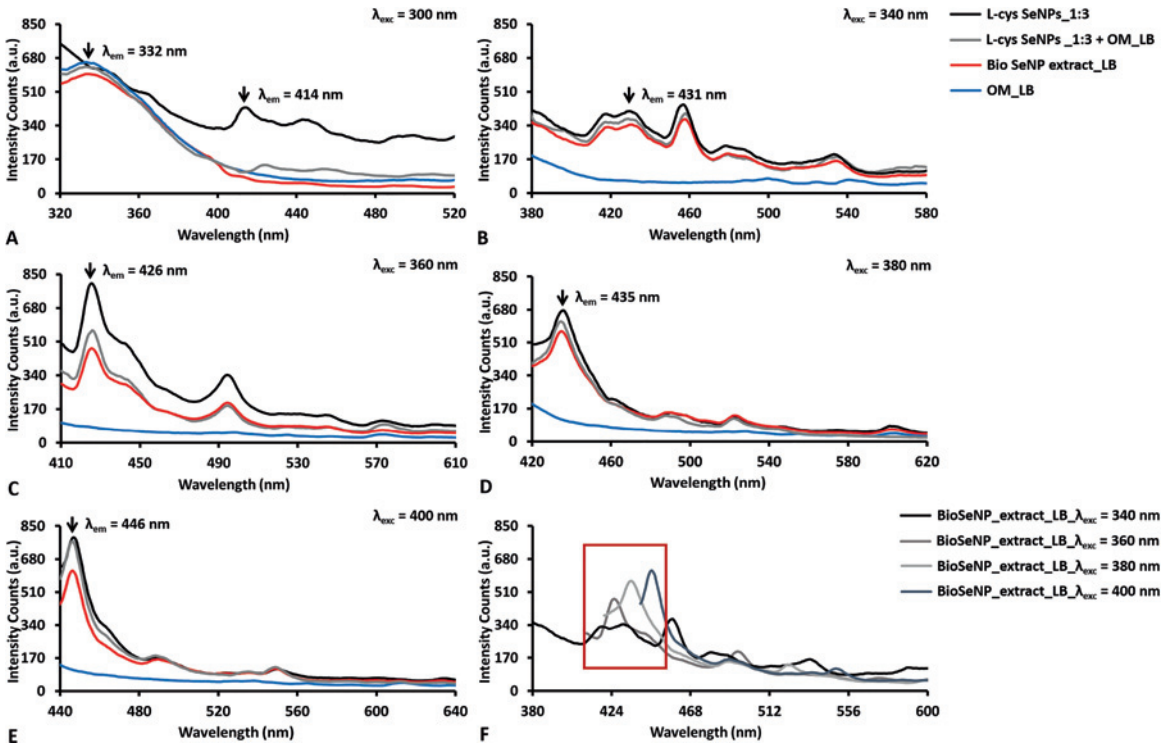

Figure 5: Emission photoluminescence spectra collected for SeNPs of ca. 50 nm as average diameter (i.e., L-cys SeNPs_1:3, Bio SeNP extract_LB, and L-cys SeNPs_1:3 + OM_LB) and their corresponding OM (ie., OM_LB) upon their excitation at (A) 300, (B) 340, (C) 360, (D) 380, and (E) 400 nm. The overlap of the obtained emission spectra for BioSeNP extract_LB is reported in (F).

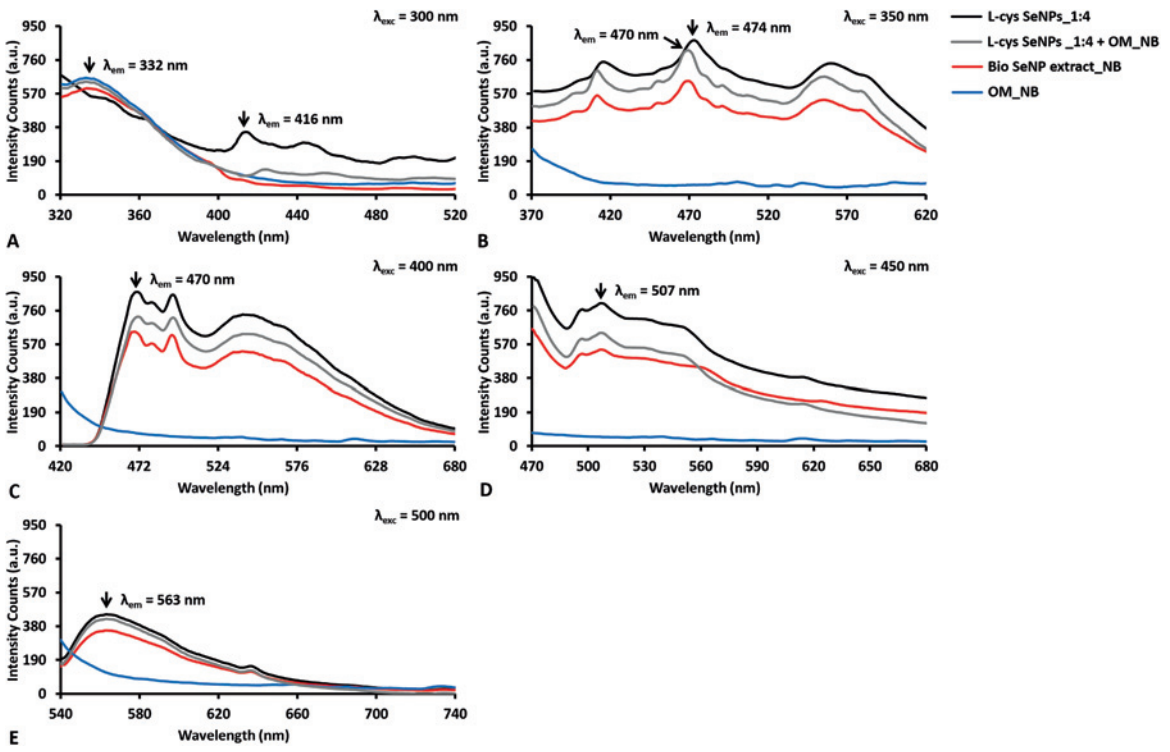

Figure 6: Emission photoluminescence spectra collected for SeNPs of ca. 100 nm as average diameter (i.e., L-cys SeNPs_1:4, Bio SeNP extract_NB, and L-cys SeNPs_1:4 + OM_NB) and their corresponding OM (i.e., OM_NB) upon excitation at (A) 300, (B) 350, (C) 400, (D) 450, and (E) 500 nm.

exciton resonance effects occur [61, 70], led to the detection of PL contributions in the 410–450 nm region (Figures 5A, 6A). Additionally, the PL excitation spectra collected for all the analyzed samples by fixing emission wavelengths (λ_{em}) at either 440 or 450 nm showed excitation peaks at ca. 260 nm (Figures S1B, S2B), suggesting the importance of the transitions from the top of the valence band to the bottom of the conduction band [70] for PL phenomena in both chemogenic and biogenic SeNPs. PL emission is greatly amplified in the case of metal NPs, where surface plasmons radiatively decay by emitting the coherent electron oscillations of SPR into photons [77]. Moreover, when NPs feature diameter smaller than the excitation wavelength ($d << \lambda_{exc}$), dipole oscillations become predominant for SPR phenomena, drastically increasing NP light absorption and emission [78]. Thus, since the $d << \lambda_{exc}$ condition was always satisfied in this study, similar phenomena (e.g., exciton resonance) occurring at the interface of SeNPs may result in the development of dipole oscillations within NPs themselves, potentially contributing to PL emission.

Other important contributors to PL properties of SeNPs are the capping agents used, being in this case either L-cysteine or the OMs. The excitation of all the samples containing the OM at 300 nm revealed a strong PL emission peak centered between 325 and 330 nm, which was not detected for chemogenic SeNPs (Figures 5A, 6A). Since the amino acid tryptophan emits fluorescence in this region [79], it is reasonable to suggest the presence of peptides and proteins in the OMs, as also reported elsewhere [6]. This evidence was further corroborated by collecting the samples' excitation spectra setting the emission wavelength (λ_{em}) at 320 nm, which showed maxima excitation peaks between 280 and 290 nm (Figures S1A, S2B). Furthermore, the OM surrounding the biogenic SeNPs, as well as L-cysteine residues present on chemogenic SeNPs, might influence their PL emission rate. Indeed, approximating SeNPs suspended in water to encapsulated oscillating dipoles [80], and considering the refractive index (n) of Se in the visible range (532 nm; arbitrary fixed) to be $n_{Se} = 3.0$, the large difference between the water refractive index ($n_w = 1.33$) and n_{Se} would result in a modest (or even close to zero) PL emission for bare NPs, as most of the light would be trapped inside the NPs themselves [16, 80]. This limited PL emission is usually compensated by using polymers with $n_w < n_p < n_{Se}$ as a coating for NPs, which simultaneously provide steric hindrance for their thermodynamic stabilization [2] and decrease the refractive index difference between NPs and water [16, 80]. PL emission of SeNPs can be also promoted by their chemical interaction with the biomolecules of the OM (proteins, lipids, and carbohydrates) [6, 57] or L-cysteine residues, determining, for instance, the generation of dipole-dipole or ionic-dipole interactions between biomolecular functional groups – e.g., amine or thiol groups – and Se at the NP surface [81]. Evidence supporting this hypothesis was previously reported [57], where Fourier-Transform Infrared (FTIR) spectroscopy of L-cys SeNPs highlighted the disappearance of the IR absorption band at 2550 cm^{-1} [57], which is typical for the stretching vibration mode of thiols (S–H) [82], suggesting the occurrence of interaction between Se and S at the NP surface. Since it has been described how SeITE02 cells biotransform SeO_3^{2-} into Se^0 through Painter-type reactions involving –SH groups [57, 83], the absence of S–H stretching vibration in the FTIR spectra of the corresponding SeNP extract [57], as well as for those recovered from other bacterial strains (i.e., *Ochrobactrum* sp. MPV1) [69], indicate that the same Se–S interaction may take place at the NP–OM interface, which could be partially responsible for PL properties of these SeNPs. It is worth noting that to better unravel the possible occurance of Se–S interactions at the NP surface, Raman spectroscopy for the detection of typical Se–S stretching vibrations is advisable [56, 84–85]; however, this aspect goes beyond the scope of the present study.

The excitation at $\lambda_{exc} > 300$ nm of all SeNP suspensions resulted in similar emission signals, while the OMs did not show any emissive contribution (Figure 5C–F, 6B–E). The PL properties were found to strongly depend on NP size [6, 71], as indicated by the differences detected in both the emission and excitation spectra registered for small (ca. 50 nm) (Figures 5B–F, Figure S1) or big (ca. 100 nm) (Figure 6B–E, Figure S2) NPs. PL emission peaks of SeNPs of ca. 50 nm in size were mostly confined to the 400–460 nm region of the spectrum upon excitation at various wavelengths, always presenting two main signal contributions between 410–426 and 430–450 nm (Figure 5F). This phenomenon was stronger at $\lambda_{exc} = 340$ nm, where two comparable emission peaks (416 and 431 nm) were detected (Figure 5B), suggesting the presence of two SeNP populations that featured different diameters (Figure 3A–C) yet were both excitable under these experimental conditions. The redshift of the excitation wavelength from 360 to 400 nm corroborated this hypothesis, as (i) one of the two signals was preponderant for PL (Figure 5C) and (ii) the two distinct emission peaks were alternatively observed (Figure 5C–E). Indeed, the emission maximum λ_{em} redshifted from 426 to 446 nm when excited at 360 or 400 nm, respectively (Figure 5C, 5E), indicating a selective excitation of diverse NP populations as a function of their size, which was supported by the detection of three PL signals centered at ca. 330, 360, and 400 nm in the

excitation spectra collected upon setting λ_{em} = 440 nm (Figure S1B). Weak PL emissions were also recorded between 480 and 600 nm, probably due to the presence of a few large SeNPs, which would be differently excited [6]. Analogous results were reported by Khalid et al. (2016) for 80 nm (average size) SeNPs, which revealed PL peaks centered at 416 and 580 nm upon excitation at 325 nm, even though their maximum emission was registered in the green–yellow portion of the spectrum [16]. The differences in PL emission may be ascribed to the diversity of the capping material surrounding these NPs, being less complex (mixture of ascorbic acid and polyvinyl alcohol) than the OM herein present on our SeNPs. Thus, the narrow PL window of SeNPs within L-cys SeNPs_1:3, Bio SeNP extract_LB and L-cys SeNPs_1:3 + OM_LB can be traced back to both (i) their small average diameters and (ii) their relative monodispersity in suspension (Figure 3A–C, Table 1), although specific "size effects" [76] appeared to be partially responsible for the diverse PL contributions observed.

To discriminate whether the observed PL emission was attributable to either fluorescence ($\tau = 10^{-9}$–10^{-6} s) or phosphorescence ($\tau = 10^{-4}$–10^{-3} s), PL lifetime (τ) measurements (Table S2) were performed on Bio SeNP extract_LB and L-cys SeNPs_1:3, as it is an intrinsic parameter of emitters that needs to be considered when investigating their potential applications [51]. PL lifetime was monitored by using the time-domain method [16, 51], and exploiting a 405 nm pulsed laser, as any contribution deriving from the biogenic extracts excited between 280 and 320 nm would be distorted by the presence of the OMs containing biomolecules able to emit light (Figure 5A–B, 6A). As a result, multiple – very short (τ_1), intermediate (τ_2), and long (τ_3) – lifetimes were detected for both biogenic and chemogenic SeNPs (Table S2), indicating that diverse SeNP populations were responsible for light emission. This phenomenon may be correlated with the strong dependence of PL lifetime on the NP size [86], as the chosen laser, along with the setting of different emission wavelengths, could have led to the excitation of diverse SeNP subpopulations, causing distinct PL emission not only in terms of λ_{em} and intensity (Figure 5) but also the lifetime (Table S2). The lifetime of NPs becomes longer as their size increases [86], therefore indicating that the longest lifetime (τ_3) was likely due to the biggest chemogenic or biogenic SeNP population capable of emitting light. These observations led also to calculate SeNP average lifetimes ($<\tau>$), which, as the set λ_{em} redshifted, gradually incremented for L-cys SeNPs_1:3 and Bio SeNP extract_LB once excited at 400 nm, going, for instance, from 2.92–3.37 ns (λ_{em} = 440 nm) to 3.63–4.92 ns (λ_{em} = 460 nm) (Table S2), further indicating the greater contribution of bigger NPs to PL emission at longer wavelengths.

The higher polydispersity observed for the samples containing large SeNPs (Figure 3D–F, Table 1) led to an even broader PL emission (Figure 6B–E) as compared to small NPs, as multiple and wide emission or excitation peaks were observed when either λ_{exc} > 300 nm (Figure 6B–E) or λ_{em} > 450 nm (Figure S2B–D) were set respectively. Indeed, PL peaks centered at ca. 420, 470, and 540 nm were detected upon excitation at 350 nm (Figure 6B), which is in line with the results obtained for biogenic extracts recovered from SeITE02 or *Ochrobactrum* sp. MPV1 cells grown in the presence of SeO_3^{2-} under metabolically controlled conditions, as well as for L-cys SeNPs of comparable sizes (between 120 and 200 nm as average diameter) [6]. The "size effects" of SeNPs on PL properties were better represented by the emission spectra collected when λ_{exc} = 400 nm, which showed PL signals in both the blue (430–490 nm) and green (495–560 nm) regions of the spectrum (Figure 6C). Particularly, the presence of SeNP populations differing in size (Figure 3D–F) led to a more structured profile featuring multiple emission peaks between 430 and 490 nm, as well as a broader PL signal in the 495–560 nm region (Figure 6C). Since an overlap of PL emission between small (Figure 5F) and big SeNPs (Figure 6C) was observed between 430 and 450 nm, it is reasonable to suggest that the signal registered in this region for chemogenic and biogenic SeNPs was attributable to NPs featuring ca. 50 nm in size, while the second feature was due to the excitation of larger NPs. Similarly to the samples containing small SeNPs (Figure 5F), increasing the excitation wavelength used (up to λ_{exc} = 500 nm) determined the disappearance of the more structured PL signal, along with a redshift of the PL emission maxima of big SeNPs (Figure 6C–E), which is in line with the results obtained in our previous study [6]. This phenomenon resulted to be the strongest when SeNPs were excited at 500 nm, which corresponded to the detection of a PL signal in the 540–630 nm region of the spectrum (Figure 6E).

Considering the broad PL emission of L-cys SeNPs_1:4 and Bio SeNP extract_NB, their lifetime measurements were performed by exploiting both 405 and 510 nm lasers and setting multiple emission wavelengths (Tables S3–S4), as suggested by the PL emission spectra collected (Figure 6). As in the case of small (ca. 50 nm) SeNPs, biogenic and chemogenic samples featuring NPs of ca. 100 nm revealed three lifetimes – exception made for Bio SeNP extract_NB and L-cys SeNPs_1:4 in Table S3, which featured only two –, indicating that the broad PL contribution was to be traced back to the polydispersity of NPs [86]. Nevertheless, the presence of larger SeNPs resulted in the detection of longer average lifetimes (up to 6.06 ns) (Table S3) as compared to L-cys SeNPs_1:3 and Bio SeNP extract_LB.

Overall, the differences observed in $<\tau>$ values calculated for chemogenic and biogenic SeNPs might be

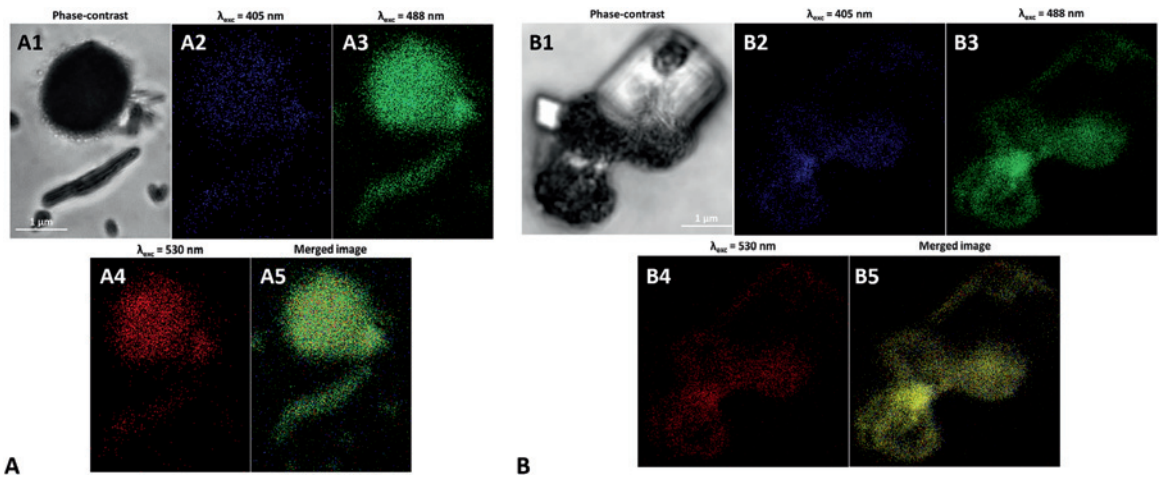

Figure 7: Super Resolution Confocal Microscopy images of (A) L-cys SeNPs_1:4 and (B) Bio SeNP extract_NB upon their excitation at (A2 and B2) 405, (A3 and B3) 488, and (A4 and B4) 530 nm. In (A1) and (B1) the phase contrast images of the samples are reported, while (A5) and (B5) show the photoluminescence merged images.

attributed to a quenching effect exerted by the OM on NPs within the biogenic extracts, which would decrease their PL lifetime, as shown in Tables S2–S3. This phenomenon was not detected upon excitation of L-cys SeNPs_1:4 and Bio SeNP extract_NB at 510 nm, which instead featured comparable average lifetimes (Table S4), likely because of the low – or even absent – optical contribution of the OM in this region of the spectrum, as also indicated by the absorbance spectra collected (Figure 4A–B).

Since the PL average lifetime was always less than 10 ns for both biogenic and chemogenic SeNPs (Tables S2–S4), fluorescence appeared to be the emission phenomenon occurring for these samples, as reported elsewhere [16]. Besides, the fluorescence lifetimes here measured were comparable to those of the most commonly used fluorophores [51], further suggesting the suitability of Bio SeNP extracts and L-cys SeNPs as bio-imaging tools [6]. Particularly, the average lifetime of Bio SeNP extract_NB and L-cys SeNPs_1:4 excited at 510 nm upon the setting of λ_{em} = 620 nm showed values ($<\tau>$ = 4.50 ns) (Table S4) similar to those reported for SeNPs stabilized by PVA [16], supporting both the experimental results and the potential application of these SeNPs as bio-markers for fluorescence measurements, such as Fluorescence Lifetime Microscopy (FLIM).

3.4 Super resolution-confocal laser scanning microscopy of biogenic SeNP extracts and chemogenic SeNPs

The potentiality of either chemogenic or biogenic SeNPs with 100 nm average diameter (i.e., L-cys SeNPs_1:4 and Bio SeNP extract_NB) as innovative yet effective PL tool was further investigated by performing SR-CLSM (Figure 7), as these NPs showed PL emission (Figure 6E) in the region of the spectrum (λ_{em} > 550 nm) where fluorescence contribution from biological components is absent. PL properties of SeNPs were monitored by fixing λ_{exc} at 405 (Figure 7A2, 7B2), 488 (Figure 7A3, 7B3) and 530 nm (Figure 7A4, 7B4), and the emission was collected in the blue (430–490 nm), green (495–560 nm) and red (600–750 nm) regions of the spectrum, respectively.

The highest intensity of emitted light was observed for both biogenic and chemogenic SeNPs upon excitation at 488 nm, which highlighted a strong green (495–560 nm) PL emission (Figure 7A3, 7B3), while at lower excitation wavelengths (λ_{exc} = 405 nm) a weaker yet present signal in the blue region of the spectrum was recorded (Figure 7A2, 7B2). PL emission was also detected upon NP excitation at 530 nm (Figure 7A4, 7B4), which is in line with the results showed by Khalid and co-workers [16]. However, this PL signal resulted to be the weakest among those unveiled, likely due to the lower number of NPs able to emit light between 600 and 750 nm, according to the PL emission and excitation spectra collected (Figure 6E, S2E–F). Finally, the merged images revealed an overlapping of PL signals upon SeNP excitation at various wavelengths (Figure 7A5, 7B5); the phase-contrast images (Figure 7A1, 7B1) highlighted how the PL emission observed derived solely from SeNPs present within the samples, as any NPs-free structure in the background was not able to emit PL as a function of the excitation wavelengths tested.

4 Conclusion

The physical and chemical properties combined with the low intrinsic toxicity of nanoscaled Se empower its use for the generation of *green* and smart high-tech products. The present study further highlights this aspect by deciphering the dependency of both biogenic and chemogenic SeNP photoluminescence properties on the NP size and polydispersity. Indeed, different bacterial growth conditions gave rise to diverse SeNP populations, which displayed a tunable photoluminescence emission, ranging from the blue to the red region of the visible-light spectrum, comparable to that of chemogenic NPs. Besides, it is noteworthy to mention the ability of both biogenic and chemogenic SeNPs to emit fluorescence beyond the so-called biological window, therefore implying their application as markers for (bio)imaging since any sort of interference with fluorescence deriving from biological components would be avoided. These SeNPs also showed a photoluminescence lifetime similar to that of the most commonly used fluorophores. Thus, this study contributes to broadening the current knowledge about biogenic SeNPs, opening, on the one hand, new avenues for their applications and, on the other, to better address their functioning as antimicrobial, anticancer, and antioxidant agents.

Acknowledgments: We gratefully acknowledge the Natural Sciences and Engineering Research Council (NSERC Discovery Grant no. RGPIN/04811-2015) for the funding, as well as the National Interuniversity Consortium of Materials Science and Technology (INSTM), and MIUR for the PON Project on Research and Innovation 2012–2020 (Attraction and International Mobility – AIM1808223). Prof. Silvia Lampis and Prof. Giovanni Vallini (University of Verona, Italy) are also acknowledged for granting the use of the bacterial strain *Stenotrophomonas maltophilia* SeITE02. Finally, the Microscopy and Imaging Facility (MIF) of the University of Calgary (Canada) and the technological platform for tissue, theragnostic and oncological engineer of the Rizzoli Orthopedic Institute (IOR) are acknowledged for accessing the TEM and SR-CLSM instruments, respectively.

Author contribution: All the authors have accepted responsibility for the entire content of this submitted manuscript and approved submission.

Research funding: None declared.

Conflict of interest statement: The authors declare that there are no conflicts of interest related to this article.

References

[1] A. G. Ingale, and A. N. Chaudhari, “Biogenic synthesis of nanoparticles and the potential applications: an eco-friendly approach,” *J. Nanomed. Nanotechnol.*, vol. 4, p. 165, 2013.

[2] E. Piacenza, A. Presentato, and R. J. Turner, “Stability of biogenic metal(loid) nanomaterials related to the colloidal stabilization theory of chemical nanostructures,” *Crit. Rev. Biotechnol.*, vol. 25, pp. 1–20, 2018.

[3] S. A. Wadhwani, U. U. Shedbalkar, R. Singh, and B. A. Chopade, “Biogenic selenium nanoparticles: current status and future prospects,” *Appl. Microbiol. Biotechnol.*, vol. 100, pp. 2555–2566, 2016.

[4] S. Shoeibi, P. Mozdziak, and A. Golkar-Narenji, “Biogenesis of selenium nanoparticles using green chemistry,” *Top Curr. Chem.*, vol. 375, p. 88, 2017.

[5] A. Presentato, E. Piacenza, M. Anikovskiy, M. Cappelletti, D. Zannoni, and R. J. Turner, “Biosynthesis of selenium nanoparticles and nanorods as a product of selenite bioconversion by the aerobic bacterium *Rhodococcus aetherivorans BCP1*,” *New Biotechnol.*, vol. 41, pp. 1–8, 2018.

[6] E. Piacenza, A. Presentato, E. Ambrosi, et al., “Physical-chemical properties of biogenic selenium nanostructures produced by *Stenotrophomonas maltophilia* SeITE02 and *Ochrobactrum* sp. MPV1 strains,” *Front Microbiol.*, vol. 9, p. 3178, 2018.

[7] E. Piacenza, A. Presentato, M. Bardelli, S. Lampis, G. Vallini, and R. J. Turner, “Influence of bacterial physiology on processing of selenite, biogenesis of nanomaterials and their thermodynamic stability,” *Molecules.*, vol. 24, p. 2532, 2019.

[8] W. N. Haynes, “Section 4, properties of the elements and inorganic compounds,” in *Handbook of Chemistry and Physics*, W. N. Haynes, D. R. Lide, and T. J. Bruno, Eds. 95th ed. Boca Raton, FL, USA, CRC Press/Taylor and Francis, 2014, pp. 115–120.

[9] X. C. Song, Y. Zhao, Y. F. Zheng, E. Yang, W. Q. Chen, and Y. Q. Fang, “Fabrication of Se/C coaxial nanocables through a novel solution process,” *J. Phys. Chem. C.*, vol. 112, pp. 5352–5355, 2008.

[10] O. Vidal, B. Goffé, and N. Arndt, “Metals for a low-carbon society,” *Nat. Geosci.*, vol. 6, pp. 894–896, 2013.

[11] T. Hennebel, N. Boon, S. Maes, and M. Lenz, “Biotechnologies for critical raw material recovery from primary and secondary sources: R&D priorities and future perspectives,” *New Biotechnol.*, vol. 32, pp. 121–127, 2015.

[12] S. Ilyas, M. S. Kim, J. C. Lee, A. Jabeen, and H. N. Bhatti, “Bioreclamation of strategic and energy critical metals from secondary resources,” *Metals.*, vol. 7, p. 207, 2017.

[13] S. Chaudhari, A. Umar, and S. K. Mehta, “Selenium nanomaterials: an overview of recent developments in synthesis, properties and potential applications,” *Progr. Mater. Sci.*, vol. 83, pp. 270–329, 2016.

[14] S. Chawla, “Chapter 37, nanoparticles and fluorescence,” in *Handbook of Nanoparticles*. M. Aliofkhazraei, Ed., London, UK, Springer International Publishing, 2016, pp. 961–984.

[15] S. Tomljenovic-Hanic, A. J. O. Connor, and W. S. Morrison, “Nanoparticles in biomedicine: let there be intrinsic light,” *Biomed. Res. Clin. Prac.*, vol. 3, pp. 1–2, 2018.

[16] A. Khalid, P. A. Tran, R. Norello, D. A. Simpson, A. J. O’Connor, and S. Tomljenovic-Hanic, “Intrinsic fluorescence of selenium

nanoparticles for cellular imaging applications," *Nanoscale.*, vol. 8, pp. 3376–3385, 2016.

[17] R. Hassanien, A. A. I. Abed-Elmageed, and D. Z. Husein, "Eco-friendly approach to synthesize selenium nanoparticles: photocatalytic degradation of sunset yellow azo dye, and anticancer activity," *Chemistry Select.*, vol. 4, pp. 9018–9026, 2019.

[18] E. Piacenza, A. Presentato, E. Zonaro, S. Lampis, G. Vallini, and R. J. Turner, "Selenium and tellurium nanomaterials," *Phys. Sci. Rev.*, vol. 3, p. 20170100, 2018.

[19] N. Singh, P. Saha, K. Rajkumar, and J. Abraham, "Biosynthesis of silver and selenium nanoparticles by *Bacillus* sp. JAPSK2 and evaluation of antimicrobial activity," *Der. Pharm. Lett.*, vol. 6, pp. 175–181, 2014.

[20] N. Srivastava, and M. Mukhopadhyay, "Green synthesis and structural characterization of selenium nanoparticles and assessment of their antimicrobial property," *Bioprocess Biosyst. Eng.*, vol. 38, pp. 1723–1730, 2015.

[21] E. Zonaro, S. Lampis, R. J. Turner, S. J. S. Qazi and G. Vallini, "Biogenic selenium and tellurium nanoparticles synthesized by environmental microbial isolates efficaciously inhibit bacterial planktonic cultures and biofilms," *Front Microbiol.*, vol. 6, p. 584, 2015.

[22] E. Cremonini, E. Zonaro, M. Donini, et al., "Biogenic selenium nanoparticles: characterization, antimicrobial activity and effects on human dendritic cells and fibroblast," *Microb. Biotechnol.*, vol. 9, pp. 758–771, 2016.

[23] E. Cremonini, M. Boaretti, I. Vandecandelaere, et al., "Biogenic selenium nanoparticles synthesized by *Stenotrophomonas maltophilia* SEITE02 loose antibacterial and antibiofilm efficacy as a result of the progressive alteration of their organic coating layer," *Microb. Biotechnol.*, vol. 11, pp. 1037–1047, 2018.

[24] E. Piacenza, A. Presentato, E. Zonaro, et al., "Antimicrobial activity of biogenically produced spherical Se-nanomaterials embedded in organic material against *Pseudomonas aeruginosa* and *Staphylococcus aureus* strains on hydroxyapatite-coated surfaces," *Microb. Biotechnol.*, vol. 10, pp. 804–818, 2017.

[25] N. Parsameher, S. Rezaei, S. Khodavasiy, et al., "Effect of biogenic selenium nanoparticles on ERG11 and CDR1 gene expression in both fluconazole-resistant and -susceptible *Candida albicans* isolates," *Curr. Med. Mycol.*, vol. 3, pp. 16–20, 2017.

[26] S. Ratnakomala, N. F. Sari, F. Fahrurrozi, and P. Lisdiyanti, "Antimicrobial activity of selenium nanoparticles synthesized by *actinomycetes* isolated from lombok island Soil Samples," *J. Kim. Terap. Indones.*, vol. 20, pp. 8–15, 2018.

[27] C. Xu, Y. Guo, L. Qiao, L. Ma, Y. Cheng, and A. Roman, "Biogenic synthesis of novel functionalized selenium nanoparticles by *Lactobacillus casei* ATCC 393 and its protective effects on intestinal barrier dysfunction caused by enterotoxigenic *Escherichia coli* K88," *Front Microbiol.*, vol. 9, p. 1129, 2018.

[28] P. Sonkusre, R. Nanduri, P. Gupta, and S. S. Cameotra, "Improved extraction of intracellular biogenic selenium nanoparticles and their specificity for cancer chemoprevention," *J. Nanomed. Nanotechnol.*, vol. 5, p. 194, 2014.

[29] P. Sonkusre, and S. S. Cameotra, "Biogenic selenium nanoparticles inhibit *Staphylococcus aureus* adherence on different surfaces," *Colloids Surf. B. Biointerfaces*, vol. 136, pp. 1051–1057, 2015.

[30] P. Sonkusre, and S. S. Cameotra, "Biogenic selenium nanoparticles induce ROS-mediated necroptosis in PC-3 cancer cells through TNF activation," *J. Nanobiotechnol.*, vol. 15, p. 43, 2017.

[31] M. H. Yazdi, M. Mahdavi, E. Faghfuri, et al., "Th1 immune response induction by biogenic selenium nanoparticles in mice with breast cancer: preliminary vaccine model," *Iran J. Biotech.*, vol. 13, Art no. e1056, 2015.

[32] M. S. Ahmad, M. M. Yasser, E. N. Sholkamy, A. M. Ali, and M. M. Mehanni, "Anticancer activity of biostabilized selenium nanorods synthesized by *Streptomyces bikiniensis* strain Ess_amA-1," *Int. J. Nanomedicine*, vol. 10, pp. 3389–3401, 2015.

[33] P. Bao, K. Q. Xiao, H. J. Wang, et al., "Characterization and potential applications of a selenium nanoparticle producing and Nitrate reducing bacterium *Bacillus oryziterrae* sp. nov," *Sci. Rep.*, vol. 6, p. 34054, 2016.

[34] S. A. Wadhwani, M. Gorain, P. Banerjee, et al., "Green synthesis of selenium nanoparticles using *Acinetobacter* sp. SW30: optimization, characterization and its anticancer activity in breast cancer cells," *Int. J. Nanomed.*, pp. 6841–6855, 2017, https://doi.org/10.2147/ijn.s139212.

[35] P. Sonkurse, "Specificity of biogenic selenium nanoparticles for prostate cancer therapy with reduced risk of toxicity: an *in vitro* and *in vivo* study," *Front Oncol.*, vol. 9, p. 1541, 2020.

[36] H. W. Tan, H. Y. Mo, A. T. Y. Lau, and Y. M. Xu, "Selenium species: current status and potentials in cancer prevention and therapy," *Int. J. Mol. Sci.*, vol. 20, p. 75, 2019.

[37] A. Khurana, S. Tekula, M. A. Saifi, P. Venkatesh and C. Godugu, "Therapeutic applications of selenium nanoparticles," *Biomed. Pharmacother*, vol. 111, pp. 802–812, 2019.

[38] H. Vahidi, H. Barabadi, and M. Saravanan, "Emerging selenium nanoparticles to combat cancer: a systematic review," *J. Clust. Sci.*, vol. 31, pp. 301–309, 2020.

[39] S. K. Torres, V. L. Campos, C. G. Leon, et al., "Biosynthesis of selenium nanoparticles by *Pantoea agglomerans* and their antioxidant activity," *J. Nanopart. Res.*, vol. 14, p. 1236, 2012.

[40] H. Forootanfar, M. Adeli-Sardou, M. Nikkhoo, et al., "Antioxidant and cytotoxic effect of biologically synthesized selenium nanoparticles in comparison to selenium dioxide," *J. Trace Elem. Med. Biol.*, vol. 28, pp. 75–79, 2014.

[41] C. Xu, L. Qiao, Y. Guo, L. Ma, and Y. Cheng, "Preparation, characteristics and antioxidant activity of polysaccharides and proteins-capped selenium nanoparticles synthesized by *Lactobacillus casei* ATCC 393," *Carbohydr. Polym.*, vol. 195, pp. 576–585, 2018.

[42] M. Shakibaie, A. R. Shahverdi, M. A. Faramarzi, G. R. Hassanzadeh, H. R. Rahimi, and O. Sabzevari, "Acute and subacute toxicity of novel biogenic selenium nanoparticles in mice," *Pharm. Biol.*, vol. 51, pp. 58–63, 2013.

[43] T. Wang, L. Yang, B. Zhang, and J. Liu, "Extracellular biosynthesis and transformation of selenium nanoparticles and application in H2O2 biosensor," *Colloids Surf. B. Bionterfaces*, vol. 80, pp. 94–102, 2010.

[44] A. Ameri, M. Shakibaie, A. Ameri, A. Faramarzi, B. Amir-Heidari, and H. Forootanfar, "Photocatalytic decolorization of bromothymol blue using biogenic selenium nanoparticles synthesized by terrestrial actinomycete *Streptomyces griseobrunneus* strain FSHH12," *Desalin. Water Treat.*, vol. 57, pp. 21552–21563, 2016.

[45] L. Che, Y. Dong, M. Wu, Y. Zhao, L. Liu, and H. Zhou, "Characterization of Selenite reduction by *lysinibacillus* sp. ZYM-1 and photocatalytic performance of biogenic selenium nanospheres," *ACS Sustainable Chem. Eng.*, vol. 5, pp. 2535–2543, 2017.
[46] R. M. Tripathi, P. Hameed, R. P. Rao, N. Shrivastava, J. Mittal, and S. Mohapatra, "Biosynthesis of highly stable fluorescent selenium nanoparticles and the evaluation of their photocatalytic degradation of dye," *BioNanoScience* 2020, https://doi.org/10.1007/s12668-020-00718-0.
[47] S. Di Gregorio, S. Lampis, and G. Vallini, "Selenite precipitation by a rhizospheric strain of *Stenotrophomonas* sp. isolated from the root system of *Astragalus bisulcatus*: a biotechnological perspective," *Environ. Int.*, vol. 31, pp. 233–241, 2005.
[48] Q. Li, T. Chen, F. Yang, J. Liu, and W. Zheng, "Facile and controllable one-step fabrication of selenium nanoparticles assisted by L-cysteine," *Mater. Lett.*, vol. 64, pp. 614–617, 2010.
[49] A. Presentato, E. Piacenza, M. Anikovskiy, M. Cappelletti, D. Zannoni, and R. J. Turner, "*Rhodococcus aetherivorans* BCP1 as cell factory for the production of intracellular tellurium nanorods under aerobic conditions," *Micro. Cell. Fact.*, vol. 15, p. 204, 2016.
[50] A. Presentato, E. Piacenza, A. Darbandi, et al., "Assembly, growth and conductive properties of tellurium nanorods produced by *Rhodococcus aetherivorans* BCP1," *Sci. Rep.*, vol. 8, p. 3923, 2018.
[51] X. Meng, X. Wang, Z. Cheng, et al., "Photoluminescence lifetime of black phosphorus nanoparticles and their applications in live cell imaging," *Appl. Mater. Interfaces*, vol. 10, pp. 31136–31145, 2018.
[52] C. Ripoll, A. Orte, L. Paniza, and M. J. Ruedas-Rama, "A quantum dot-based FLIM glucose nanosensor," *Sensors*, vol. 19, p. 4992, 2019.
[53] A. Muller, D. Behsnilian, E. Walz, V. Graf, L. Hogekamp, and R. Greiner, "Effect of culture medium on the extracellular synthesis of silver nanoparticles using *Klebsiella pneumoniae, Escherichia coli* and *Pseudomonas jessinii*," *Biocatal. Agric. Biotechnol.*, vol. 6, pp. 107–115, 2016.
[54] K. Luo, S. Jung, K. H. Park, and Y. R. Kim, "Microbial biosynthesis of silver nanoparticles in different culture media," *J. Agric. Food Chem.*, vol. 66, pp. 957–962, 2018.
[55] E. Baltazar-Encarnacion, C. E. Escarcega-Gonzalez, X. G. Vasto-Anzaldo, M. E. Cantú-Cárdenas, and J. R. Morones-Ramirez, "Silver nanoparticles synthesized through green methods using *Escherichia coli* top 10 (Ec-Ts) growth culture medium exhibit antimicrobial properties against nongrowing bacterial Strains," *J. Nanomater.*, p. 4637325, 2019.
[56] A. V. Tugarova, P. V. Mamchenkova, V. A. Khanadeev, and A. A. Kamnev, "Selenite reduction by the rhizobacterium *Azospirillum brasilense*, synthesis of extracellular selenium nanoparticles and their characterisation," *New Biotechnol.*, vol. 58, pp. 17–24, 2020.
[57] S. Lampis, E. Zonaro, C. Bertolini, et al., "Selenite biotransformation and detoxification by *Stenotrophomonas maltophilia* SeITE02: novel clues on the route to bacterial biogenesis of selenium nanoparticles," *J. Haz. Mat.*, vol. 324, pp. 3–14, 2017.
[58] G. Gonzales-Gil, P. N. L. Lens, and P. E. Saikaly, "Selenite reduction by anaerobic microbial aggregates: microbial community structure, and proteins associated to the produced selenium spheres," *Front Microbiol.*, vol. 7, p. 571, 2016.
[59] A. V. Tugarova, and A. A. Kamnev, " Proteins in microbial synthesis of selenium nanoparticles," *Talanta*, vol. 174, pp. 539–547, 2017.
[60] M. Kerker. *The Scattering of Light and Other Electromagnetic Radiation*. NY, USA, Academic Press, 1969.
[61] S. K. Islam, M. A. Sohel, and J. R. Lomabrdi, "Coupled exciton and charge transfer resonances in the Raman enhancement of phonon modes of CdSe quantum dots (QDs)," *J. Phys. Chem. C.*, vol. 118, pp. 19415–19421, 2014.
[62] A. A. Kamnev, P. V. Mamchenkova, Y. A. Dyatlova, and A. V. Tugarova, "FTIR spectroscopy studies of selenite reduction by cells of the rhizobacterium *Azospirillum brasilense* Sp7 and the formation of selenium nanoparticles," *J. Mol. Struct.*, vol. 1140, pp. 106–112, 2017.
[63] D. Xu, L. Yang, Y. Wang, G. Wang, C. Rensing, and S. Zheng, "Proteins enriched in charged amino acids control the formation and stabilization of selenium nanoparticles in *Comamonas testosteroni* S44," *Sci. Rep.*, vol. 8, p. 4766, 2018.
[64] L. Y. Cruz, D. Wang, and J. Liu, "Biosynthesis of selenium nanoparticles, characterization and X-ray induced radiotherapy for the treatment of lung cancer with interstitial lung disease," *J. Photoch. Photobio. B.*, vol. 191, pp. 123–127, 2019.
[65] M. Yazhiniprabha, and B. Vaseeharan, "*In vitro* and *in vivo* toxicity assessment of selenium nanoparticles with significant larvicidal and bacteriostatic properties," *Mater. Sci. Eng. C.*, vol. 103, p. 109763, 2019.
[66] Z. H. Lin, and C. R. Wang, "Evidence on the size-dependent absorption spectral evolution of selenium nanoparticles," *Mat. Chem. Phys.*, vol. 92, pp. 591–594, 2005.
[67] C. P. Shah, C. Dwivedi, K. K. Singh, M. Kumar, and P. N. Bajaj, "Riley oxidation: a forgotten name reaction for synthesis of selenium nanoparticles," *Mater. Res. Bull.*, vol. 45, pp. 1213–1217, 2010.
[68] C. Dwivedi, C. P. Shah, K. Singh, M. Kumar, and P. N. Bajaj, "An organic acid-induced synthesis and characterization of selenium nanoparticles," *J. Nanotechnol.*, pp. 651971, 2011.
[69] W. Chen, Y. Li, S. Yang, L. Yue, Q. Jiang, and W. Xia, "Synthesis and antioxidant properties of chitosan and carboxymethyl chitosan-stabilized selenium nanoparticles," *Carbohydr. Polym.*, vol. 132, pp. 574–581, 2015.
[70] S. C. Singh, S. K. Mishra, R. K. Srivastava, and R. Gopal, "Optical properties of selenium quantum dots produced with laser irradiation of water suspended Se nanoparticles," *J. Phys. Chem. C.*, vol. 114, p. 17374, 2010.
[71] A. E. Raevskaya, A. L. Stroyuk, S. Y. Kuchmiy, V. M. Dzhagan, D. R. T. Zahn, and S. Schulze, "Annealing-induced structural transformation of gelatin-capped Se nanoparticles," *Solid State Commun.*, vol. 145, pp. 288–292, 2008.
[72] N. Mollania, R. Tayebee, and F. Narenji-Sani, "An environmentally benign method for the biosynthesis of stable selenium nanoparticles," *Res. Chem. Intermed.*, vol. 42, pp. 4253–4271, 2016.
[73] A. R. Ingole, S. R. Thakare, N. T. Khati, A. V. Wankhade, and D. K. Burghate, "Green synthesis of selenium nanoparticles under ambient condition," *Chalcogenide Lett.*, vol. 7, pp. 485–489, 2010.
[74] E. Zonaro, E. Piacenza, A. Presentato, et al., "*Ochrobactrum* sp. MPV1 from a dump of roasted pyrites can be exploited as

bacterial catalyst for the biogenesis of selenium and tellurium nanoparticles," *Micr. Cell. Fact.*, vol. 16, p. 215, 2017.
[75] F. X. Schmid, "Biological macromolecules: UV-visible spectrophotometry," *ELS*, pp. 1–4, 2001.
[76] M. V. Lesnichaya, R. Shendrik, and B. G. Sukhov, "Relation between excitation dependent luminescence and particle size distributions for the selenium nanoparticles in κ-carrageenan shell," *J. Luminesc.*, pp. 305–313, 2019, https://doi.org/10.1016/j.jlumin.2019.03.056.
[77] S. A. Maier, "Enhancement of emissive processes and nonlinearities," in *Plasmonics: Fundamentals and Applications*, S. A. Maier, Ed., NY, USA, Springer, 2007, pp. 159–176.
[78] U. Kreibig, and M. Vollmer, "Experimental results and discussion," in *Optical Properties of Metal Clusters*, U. Kreibig, and M. Vollmer, Eds., NY, USA, Springer Series in Material Science, 1995, pp. 275–436.
[79] J. R. Lakowicz, "Chapter 16, protein fluorescence," in *Principles of Fluorescence Spectroscopy*, J. R. Lakowicz, Ed., NY, USA, Springer Science C Business Media, 1999, pp. 446–485.
[80] K. Chung, and S. Tomljenovic-Hanic, "Emission properties of fluorescent nanoparticles determined by their optical environment," *Nanomaterials*, vol. 5, pp. 895–905, 2015.
[81] A. Salem, E. Saion, N. M. Al-Hada, et al., "Synthesis and characterization of CdSe nanoparticles via thermal treatment technique," *Res. Phys.*, vol. 7, pp. 1556–1562, 2017.
[82] R. A. Nyquist, "Chapter 4, thiols, Sulfides and disulfides, alkanethiols, and alkanedithiols (S-H stretching)," in *Interpreting Infrared, Raman, and Nuclear Magnetic Resonance Spectra*, R. A. Nyquist, Ed., NY, USA, Academic Press, 2001, pp. 65–83.
[83] P. Antonioli, S. Lampis, I. Chesini, et al., "*Stenotrophomonas maltophilia* SeITE02, a new bacterial strain suitable for bioremediation of selenite-contaminated environmental matrices," *Appl. Environ. Microbiol.*, vol. 73, pp. 6854–6863, 2007.
[84] M. Vogel, S. Fischer, A. Maffert, et al., "Biotransformation and detoxification of selenite by microbial biogenesis of selenium-sulfur nanoparticles," *J. Haz. Mat.*, vol. 344, pp. 749–757, 2018.
[85] A. S. Eswayah, N. Hondow, A. C. Scheinost, et al., "Methyl selenol as a precursor in selenite reduction to Se/S species by methane-oxidizing bacteria," *Appl. Environ. Microbiol.*, vol. 85, pp. e01379–19, 2019.
[86] K. K. Chattopadhyay, and N. K. Das, "Chapter 11, Size-dependent optical properties of nanoparticles analyzed by spectroscopic ellipsometry," in *Handbook of Nanoparticles*, M. Aliofkhazraei, Ed., London, UK, Springer International Publishing, 2016, pp. 265–294.

Supplementary Material: The online version of this article offers supplementary material https://doi.org/10.1515/nanoph-2020-0039.